COBEM 2023 27TH INTERNATIONAL CONGRESS OF MECHANICAL ENGINEERING

ABCM Brazilian Society of Mechanical Sciences and Engineering
27th ABCM International Congress of Mechanical Engineering
December 04-08, 2023, Florianópolis-SC, Brazil

COB-2023-1863
PRE AND POST WELDING GEOMETRIC DEVIATION MEASUREMENT METHOD IN STAINLESS STEEL 304 WELDED BY FCAW

Alexandre de Oliveira Dias
Universidade de São Paulo - Escola Politécnica. Av. Prof. Mello Moraes, 2231, Cidade Universitária, Butantã, São Paulo-SP.
alexandredias@usp.br
Bruno Gabriel Carneiro
Rafael Antônio Pereira da Fonseca
Raphael Silva Lins
Universidade Federal do Triângulo Mineiro – Av. Randolfo Borges Jr, 2856, Univerdecidade, Uberaba-MG.
brunogabriel.carneiro99@gmail.com; rafaelfonseca88@outlook.com.br; raphael.lins@uftm.edu.br
Marcílio Alves
Universidade de São Paulo - Escola Politécnica. Av. Prof. Mello Moraes, 2231, Cidade Universitária, Butantã, São Paulo-SP.
maralves@usp.br

Abstract. *The flux cored arc welding (FCAW) of stainless steels, due to the high rate of deposition properties and excellent resistance to impact, is possible to be applied in many industrial sectors, such as the food, chemical, and petrochemical industries, especially in equipment subject to cryogenic temperatures. Faced with this demand, this article intends to demonstrate a method of quality control in test specimens of stainless steel 304 in welding by the flux-cored wire process. The method consists of tracing specific points (X, Y) along the surface of the specimen in order to monitor deviations in flatness, straightness, and punctuality of the material before and after welding with simple deposition of a weld bead. In measurements related to the plane, a mesh with 36 points was measured. It was possible to acquire flatness, angle of inclination, squareness (ZX and YZ), and parallelism (XY), both in their respective reference lengths. In line-related measurements, 12 points were measured on a line 10mm away from one of the lateral vertices of the specimen. Thirty specimens measuring 5/8 inch x 6 inch x 2 inches were analyzed. By superimposing these surfaces, using computer-aided design (CAD) software, it was possible to quantify the deviations and verify which variables of the welding process most affected these shape deviations. The weld beads were centered and had approximate lengths of 2 inches, the welding was carried out in the flat position using a Gullco welding carriage. Voltage and current data were acquired during the process. The mass of the test specimens was weighed before and after welding, as well as the real length of the bead and the geometry (width and reinforcement). The method proved to be efficient to verify geometric deviations in scientific welding experiments and aims to demonstrate that preparatory welding methods have an influence on post-welding characteristics. The length of the weld has a strong influence on deformations since the welding energy remained.*

Keywords: *FCAW, AISI 304,E316LT1-1, welding deformation, MMC.*

1. INTRODUCTION

Industries are concerned in obtaining welding procedures combining versatility, productivity and quality, related to reduced costs in their operations, in order to guarantee the greater competitiveness in a fierce competition sector.

Among the options for welding, the tubular wire process (FCAW) has been growing in use due some peculiarities, such as ease field application (Oliveira, 2005; Starling and Modenesi, 2006; Dias, 2009; Marques, 2005).

This process allows high quality weld bead and good visual appearance. It can be used in all welding positions through adjusting the operating parameters. It also presents a high productivity, due to its high deposition rate and low spatter index, providing high deposit yield (Lima and Ferraresi, 2006).

Due to the increasing use of the tubular wire (FCAW) welding process, associated to its characteristics of high deposition rate, high efficiency and adequate mechanical properties of the welded joint, this process has been widely studied (Arun et al., 2019; Oliveira et al., 2005), because of the ease of application in the field (Oliveira, 2005).

Due to the good physical properties of austenitic stainless steels and their specific mechanical behaviors, it is necessary to make some arrangements to ensure a perfect weld; being fundamental the appropriate choice of welding process and filler metal, provided that it has compatibility in the chemical composition with the base metal (Sriba et al., 2018). Austenitic stainless steels contain high levels of nickel and other austenite-forming elements, promoting the formation of this phase, being stable at room temperature and below (Lippold and Kotecki, 2005).

In austenitic stainless steels, whose elongation values are high, these alloying elements are distributed in a single phase, making the corrosion resistance homogeneous (Senatore and Perea, 2007). The 304 series austenitic stainless steels are widely used in nuclear structure parts, automotive, as well as mechanical applications (Srivastava et al., 2018). (Kannengiesser and Kromm, 2009) and (Dey et al., 2004) concluded that, in alloys 18-8 (%Cr-%Ni), there is a greater variation of residual stresses along the width of the weld bead.

2. EXPERIMENTAL METODOLOGY

In order to optimize the parameters it was used preliminary tests for choose the best heat input (H) in a overlay welding. The FCAW process was used, stick out 15mm and retreat of 5mm at a 30 degrees torch inclination angle. The welding machine used was a Miller Dataweld 500.

The welds were made in (Fig. 2), measuring approximately 50 mm in length, exhibiting rutile slag detachable. It were used heat input (H) of 707.4 J/mm (specimen DWT 9); 728.7 J/mm (specimen DWT 10); 730,4 J/mm (specimen DWT11); 725,9 J/mm (specimen DWT12) and 757.1 J/mm (specimen DWT13). This H values were acquired by a Miller Insight Arc Agent Spec Sheet. Table 1 shows the chemical composition of Addition Metal and Base Metal. The welds were performed with protection by carbon dioxide at the face, in order to avoid contamination of the weld and minimize discontinuities and defects. The Chromium equivalent (Creq) and Nieq were calculated by the equivalent formulas WRC-1988 and WRC-1992, respectively:

$Creq = Cr + Mo + 0.7Nb$

$Nieq = Ni+35C+20N+0.25Cu$

Table 1 – Base metal and filler metal chemical compositions

	C %	Si %	Mn %	Cr %	Ni %	Mo%	S %	P %	Cu %	N%	Cr_{eq}	Ni_{eq}
AWS316LT1-1	0.027	0.50	2.10	18.50	13.3	2.20	0.013	0.028	0.17		20.7	14.29
ASTM 304	0.024	0.39	1.19	18.1	8.0	-	0.002	0.022	-	0.07	18.1	10.24

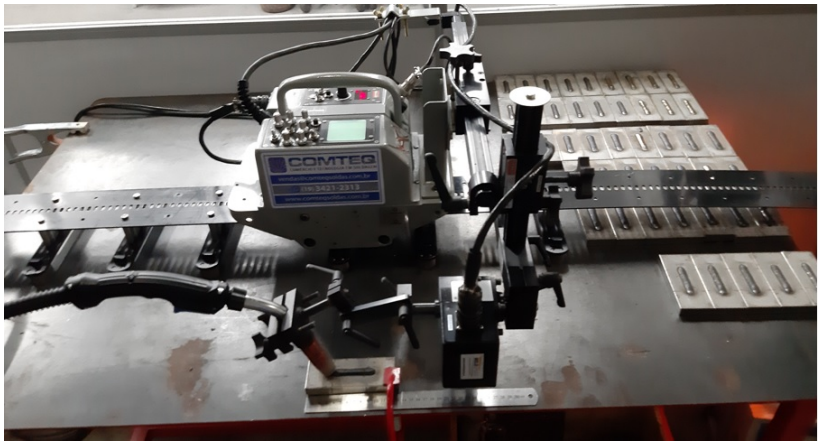

Figure 1. The Cat Gullco welding carriage in flat position.

Figure 2. Welding bead, approximately 50 mm in lenghth, with rutile slag covering the weld.

2.1 Measurement of Deformation in Coordinate Measuring Machine (CMM)

(Melo et al., 2013) evaluated the residual stress field by X-ray diffraction ($\sin^2\psi$ method) in metallic coatings from ASTM A36, with the FCAW process, and using the filler metal E308-L (Fig. 3). The influence of these stresses can be significant on longitudinal and transverse deformations.

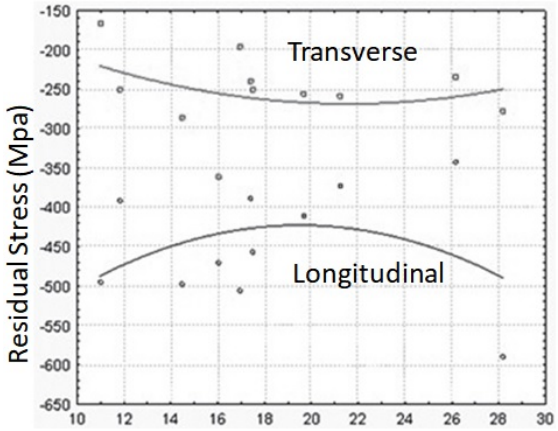

Figure 3. Welding energy influence on the level of longitudinal and transverse residual stresses and the interaction between stress levels in FCAW.

In fusion welding, there is localized heating by a heat source. During thermal cycling, the solder is subject to thermal stresses. After, incompatible voltages remain in the regions close to the weld. Incompatible stresses, including dimensional changes associated with weld metal solidification, metallurgical transformations, and plastic deformations are sources of residual stresses and distortions. When changing the welding process and parameters, the heat flux pattern also changes. Changing the heat flow pattern causes a shift in the distribution of mismatched stresses, causing changes in shrinkage and distortion. (MASUBUCHI, 1980).

According to (Barban and Gonçalves, 2013), the temperature fields obtained through thermal analysis are used as input data for the mechanical solution, where thermal expansions generate deformations. For an elastic material, its behavior can be determined through the solution of fifteen equations, three of which are equilibrium, six compatibility that relate deformations, displacements, and another six constitutive ones that involve stresses and deformations. In the analysis of residual stresses and strains, both induced by welding processes, the plastic behavior of materials is also involved.

During the welding process, strain and residual stress are influenced by the total strain. In the mechanical analysis, the same mesh configuration as in the thermal analysis can be used, except for the element type and boundary conditions (Rong et al., 2016). Normally, the increase in total strain ε̇ can be expressed as the individual components of elastic, plastic and thermal strains, calculated by:

$$\dot{\boldsymbol{\varepsilon}} = \dot{\boldsymbol{\varepsilon}}_{\mathbf{e}} + \dot{\boldsymbol{\varepsilon}}_{\mathbf{p}} + \dot{\boldsymbol{\varepsilon}}_{\mathbf{tp}} + \dot{\boldsymbol{\varepsilon}}_{\mathbf{ph}} \tag{1}$$

where $\dot{\boldsymbol{\varepsilon}}_{\mathbf{e}}$, $\dot{\boldsymbol{\varepsilon}}_{\mathbf{p}}$, $\dot{\boldsymbol{\varepsilon}}_{\mathbf{tp}}$ e $\dot{\boldsymbol{\varepsilon}}_{\mathbf{ph}}$ are the elastic, plastic, thermal and phase transformation rates, respectively.

$$\boldsymbol{\sigma}_{\mathbf{ij}} = \mathbf{C}_{\mathbf{ijkl}} (\boldsymbol{\varepsilon}_{\mathbf{kl}} - \boldsymbol{\varepsilon}^{\mathbf{p}}_{\mathbf{kl}} - \boldsymbol{\varepsilon}^{\mathbf{th}}_{\mathbf{kl}} - \boldsymbol{\varepsilon}^{\mathbf{tp}}_{\mathbf{kl}} - \boldsymbol{\varepsilon}^{\mathbf{tr}}_{\mathbf{kl}}) \tag{2}$$

where $\boldsymbol{\sigma}_{\mathbf{ij}}$, $\mathbf{C}_{\mathbf{ijkl}}$, $\boldsymbol{\varepsilon}_{\mathbf{kl}}$, $\boldsymbol{\varepsilon}^{\mathbf{p}}_{\mathbf{kl}}$, $\boldsymbol{\varepsilon}^{\mathbf{th}}_{\mathbf{kl}}$, $\boldsymbol{\varepsilon}^{\mathbf{tp}}_{\mathbf{kl}}$ e $\boldsymbol{\varepsilon}^{\mathbf{tr}}_{\mathbf{kl}}$ are the objective stress, elastic constitutive tensor, elastic strain, plastic strain, thermal strains, strain induced by plastic transformation, and strains due to metallurgical change (Barban and Gonçalves, 2013) (Vargas, 2019). The stress-elastic deformation relationship of the welded material can use Hooke's law with the dependence of temperature, Young's Modulus (E) and Poison's Coefficient (ν). The thermal stress can be taken into account through the coefficient of thermal expansion. Yield stress can be defined using the von Mises criterion (Salerno et al., 2018).

Usually the primordial parcels are elastic, thermal and have at least one inelastic effect. Furthermore, during the welding of stainless steels, as the process of phase transformation in the solid state does not occur, both in the base metal and in the molten zone, the total strain rate (Eq. 1) can be reduced to (Deng and Murakawa, 2006):

$$\dot{\boldsymbol{\varepsilon}} = \dot{\boldsymbol{\varepsilon}}_{\mathbf{e}} + \dot{\boldsymbol{\varepsilon}}_{\mathbf{p}} + \dot{\boldsymbol{\varepsilon}}_{\mathbf{tp}} \tag{3}$$

As for the measurements of distortions or deformations, these can be measured using coordinate measurement tables, in order to measure the deformations before welding (from the lamination process of the plate from which the test specimens originated) and after welding.

Various forms of specimen evaluation are used to evaluate the geometric deviation of 304 stainless steel before and after welding. Before welding, it is important to take detailed dimensional measurements of the parts to be joined. Precise measuring techniques and special equipment are used to evaluate the geometric deviation of 304 stainless steel before and after welding. Before welding, it is important to take detailed dimensional measurements of the parts to be joined.

Before welding, all parts were measured with a CMM (in a controlled environment temperature) to determine the required dimensions post-weld. After welding, the welded surfaces were again analyzed dimensionally to check for any geometric deviations. The pre-welding measurements allow the detection of misalignments and irregularities in the part and the adoption of corrective strategies before the welding process. The measurement surface mesh is shown in Figure 4. The specimens were positioned in the same place on the granite table of the Tesa micro-hite coordinate measuring machine, as shown in Fig. 5.

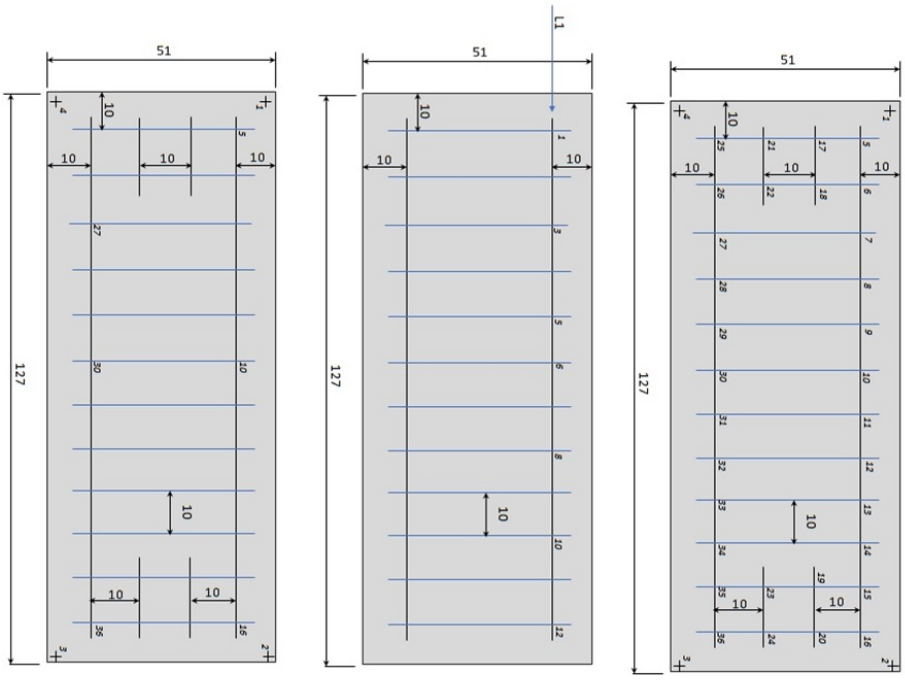

Figure 4. Superficials mesh in plane, line, and point, respectively. Specimens acording ASTM 304.

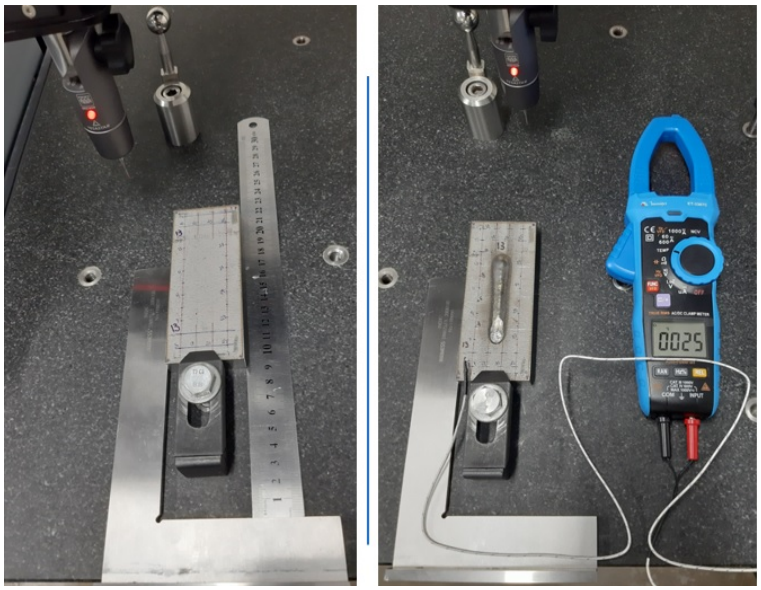

Figure 5. Schematic position specimens before and after welding.

3 RESULTS ANALYSIS

In the measurements related to the plane, 36 points were measured (Figure 4) and it was possible to acquire the flatness, the angle of inclination, squareness (ZX and YZ) and parallelism (XY), both in their respective reference lengths (Tab. 1). In line-related measurements, it was measured 12 line points, 10mm from the right end of the welding direction (Tab. 2). In point coordinates measurements, it was measured also 36 points, each one in x, y, and z coordinates (Tables 3-7).

Table 1. Metrological results for angle of inclination, squareness (ZX and YZ), and parallelism (XY). Measured of 5 specimens.

Specimen	Inclination Angle(1)		Squareness(1)		Parallelism(1)	InclinationAngle(2)		Squareness(2)		Parallelism(2)
	zx	yz	zx	yz	xy	zx	yz	zx	yz	xy
DWT 9	89.474	89.988	1.122	0.009	1.123	88.811	89.971	2.537	0.023	2.538
DWT 10	89.638	89.976	0.782	0.020	0.784	88.862	89.947	2.434	0.043	2.437
DWT 11	89.711	89.960	0.618	0.033	0.624	89.099	89.946	1.919	0.044	1.922
DWT 12	89.549	89.994	0.960	0.005	0.960	88.964	89.977	2.205	0.019	2.206
DWT 13	89.572	89.888	0.916	0.092	0.947	88.933	89.868	2.288	0.108	2.305

(1) Before welding; measured at 22°C. (2) after welding; measured at 20,6°C

Figure 6. Trend graphic of planar measurements.

Table 2. Line-related measurements. Metrological results for straightness, squareness, and parallelism.

Specimen	Straightness(1)	Squareness(1) Z	Parallelism(1) Y	Straightness (2)	Squareness(2) Z	Parallelism(2) Y
DWT 9	0.062	1.010	1.010	0.443	2.291	2.291
DWT 10	0.034	0.719	0.719	0.469	2.218	2.218
DWT 11	0.039	0.552	0.552	0.459	1.726	1.726
DWT 12	0.095	0.860	0.860	0.314	2.095	2.095
DWT 13	0.039	0.856	0.856	0.452	2.102	2.102

Before welding; measured at 23°C. (2) after welding; measured at 22,2°C

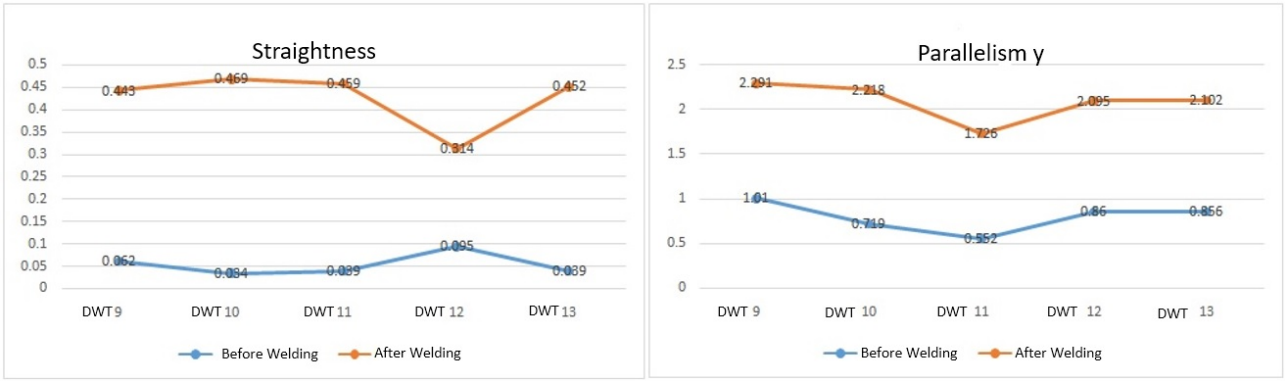

Figure 7. Trend graphic of linear measurements.

The specimens DWT 11 and DWT 12 had lower parallelism (xy and y), zx squaring and straightness (Tab.2). Having no correlation with the linear length of the bead, but correlation with the reinforcement in the center of the bead or specimen (Fig. 6). Nevertheless, the straightness was very pronounced in specimen DWT 12, which had the greatest reinforcement in the center of the weld bead (Fig. 7).

Table 3. Welding variation points in cartesian coordinates of specimen DWT9.

Point	$X^{(1)}$	$y^{(1)}$	$z^{(1)}$	$x^{(2)}$	$y^{(2)}$	$z^{(2)}$
1	112.298	10.709	-469.513	112.867	-246.398	-463.381
2	112.295	133.039	-468.814	112.879	-124.552	-460.909
3	158.058	132.678	-468.856	158.499	-124.268	-460.928
4	158.047	158.047	-469.574	158.499	-245.482	-463.426
5	120.029	17.839	-469.493	120.679	-238.649	-463.333
6	120.023	28.143	-469.407	120.686	-228.254	-463.239
7	120.021	38.202	-469.348	120.685	-218.284	-463.141
8	120.027	48.342	-469.304	120.679	-208.355	-463.030
9	120.019	58.142	-469.261	120.685	-198.460	-462.907
10	120.021	68.334	-469.177	120.682	-188.398	-462.710
11	120.017	78.167	-469.132	120.682	-178.335	-462.507
.	.	.	.	.	.	.
18	129.921	28.417	-469.119	130.637	-228.808	-463.280
.	.	.	.	.	.	.
.	.	.	.	.	.	.
26	150.892	28.257	-469.419	151.135	-228.810	-463.248
27	150.891	38.482	-469.385	151.133	-218.902	-463.159
28	150.888	48.545	-469.309	151.135	-208.845	-463.028
29	150.883	58.126	-469.273	151.131	-199.087	-462.927
30	150.889	68.551	-469.222	151.130	-188.876	-462.752
31	150.886	78.166	-469.130	151.128	-178.792	-462.509
32	150.881	88.488	-469.071	151.131	-168.949	-462.312
33	150.882	98.409	-469.027	151.132	-158.875	-462.008
34	150.885	108.195	-468.971	151.134	-149.023	-461.708
35	150.883	117.988	-468.911	151.133	-138.780	-461.374
36	150.883	127.895	-468.842	151.131	-128.258	-461.035

(1) Before welding; measured at 22°C. (2) after welding; measured at 24°C. x, y and z in millimeters.

Table 4. Welding variation points in cartesian coordinates of specimen DWT10.

Point	$X^{(1)}$	$y^{(1)}$	$z^{(1)}$	$x^{(2)}$	$y^{(2)}$	$z^{(2)}$
1	112.814	10.350	-469.536	114.456	8.825	-475.311
2	112.813	132.492	-468.632	114.674	130.467	-472.928
.	.	.	.	.	.	.
18	130.271	27.484	-469.386	132.566	26.401	-475.158
.	.	.	.	.	.	.
35	151.433	117.560	-468.742	153.148	116.166	-473.397
36	151.436	127.691	-468.651	153.148	126.210	-473.059

(1) Before welding; measured at 22°C. (2) after welding; measured at 24°C. x, y and z in millimeters.

Table 5. Welding variation points in cartesian coordinates of specimen DWT11.

Point	$X^{(1)}$	$y^{(1)}$	$z^{(1)}$	$x^{(2)}$	$y^{(2)}$	$z^{(2)}$
1	114.043	9.823	-469.522	112.438	-245.907	-463.364
2	114.039	131.605	-468.794	112.442	-124.912	-461.474
.	.	.	.	.	.	.
18	131.351	27.398	-469.380	130.554	-228.074	-463.264
.	.	.	.	.	.	.
35	152.988	117.567	-468.851	151.534	-138.028	-461.809
36	152.986	127.811	-468.785	151.533	-126.877	-460.608

(1) Before welding; measured at 20°C. (2) after welding; measured at 26°C. x, y and z in millimeters.

Table 6. Welding variation points in cartesian coordinates of specimen DWT12.

Point	$X^{(1)}$	$y^{(1)}$	$z^{(1)}$	$x^{(2)}$	$y^{(2)}$	$z^{(2)}$
1	113.105	10.047	-469.558	113.106	-313.75	-473.046
2	113.099	131.242	-468.756	113.122	-192.41	-470.866
.	.	.	.	.	.	.
18	130.974	26.646	-469.420	131.079	-295.93	-472.866
.	.	.	.	.	.	.
35	151.555	117.487	-468.722	151.998	-206.31	-471.180
36	151.557	127.293	-468.694	151.992	-196.3	-470.909

(2) Before welding; measured at 20°C. (2) after welding; measured at 22,2°C. x, y and z in millimeters.

Table 7. Welding variation points in cartesian coordinates of specimen DWT13.

Point	$X^{(1)}$	$y^{(1)}$	$z^{(1)}$	$x^{(2)}$	$y^{(2)}$	$z^{(2)}$
1	113.379	10.282	-470.242	112.264	-246.126	-463.399
2	114.204	132.594	-469.321	112.280	-123.813	-461.091
.	.	.	.	.	.	.
18	131.282	118.234	-469.432	131.103	-228.412	-463.301
.	.	.	.	.	.	.
35	152.474	118.493	-469.491	151.378	-138.679	-461.609
36	152.471	128.115	-469.457	151.381	-128.488	-461.310

(3) Before welding; measured at 22°C. (2) after welding; measured at 20,6°C. x, y and z in millimeters.

The cartesian coordinates referring to Tables 3,4,5,6 and 7 are represented in Figures 5, 7, 9, 11 and 13.

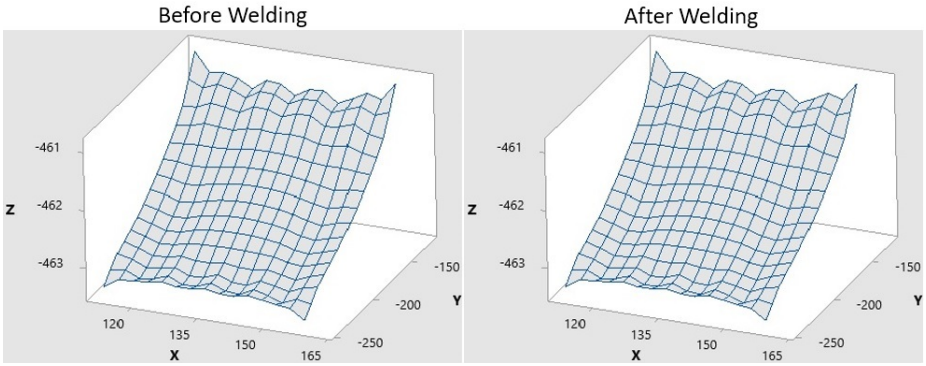

Figure 5. Surface behavior in cartesian coordinates - specimen DWT9.

Figures 6, 8, 10, 12 and 14 shows the surface overlap before and after welding of specimens (DWT9, DWT 10, DWT11, and DWT13). The yellow and red surfaces represent the specimen after welding and before welding, respectively. Both were used the Minitab Statistical® Software 2019, and SolidWorks® 2021.

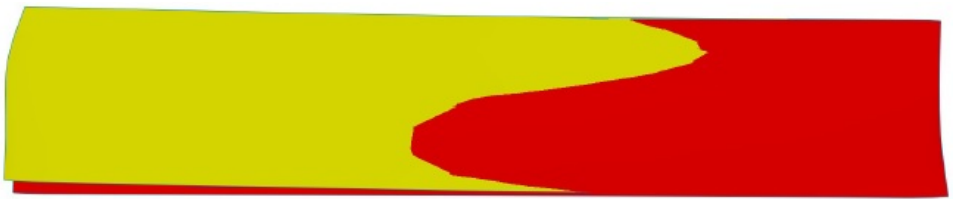

Figure 6. Overlap deformation - specimen DWT9.

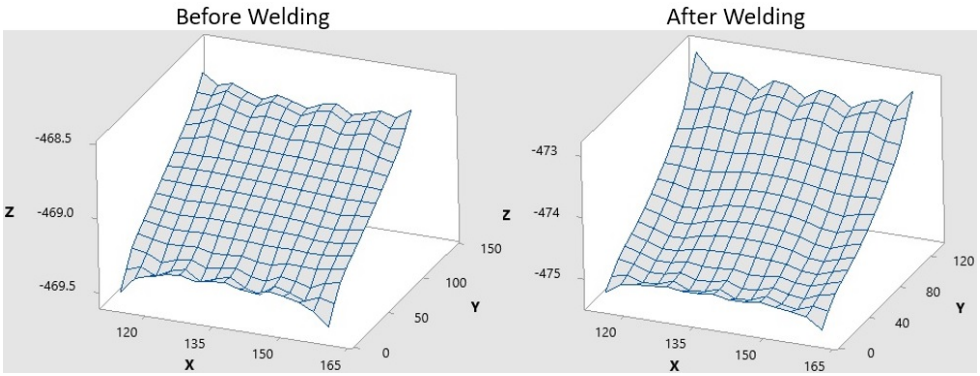

Figure 7. Surface behavior in cartesian coordinates - specimen DWT10.

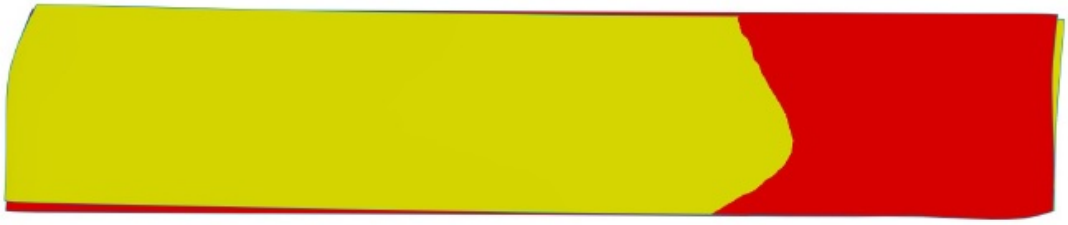

Figure 8. Overlap deformation - specimen DWT10.

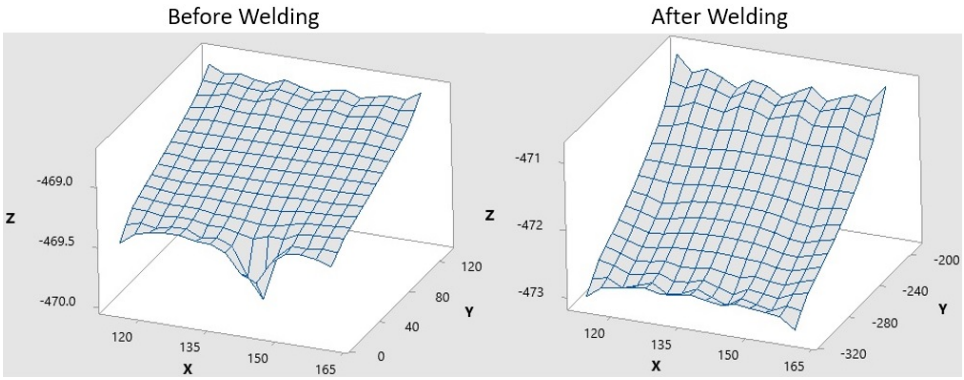

Figure 9. Surface behavior in cartesian coordinates - specimen DWT11.

Figure 10. Overlap deformation - specimen DWT11.

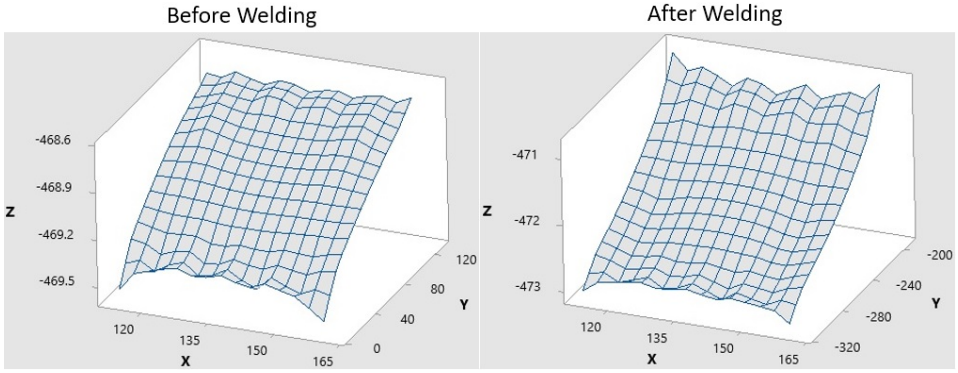

Figure 11. Surface behavior in cartesian coordinates - specimen DWT12.

Figure 12. Overlap deformation - specimen DWT12.

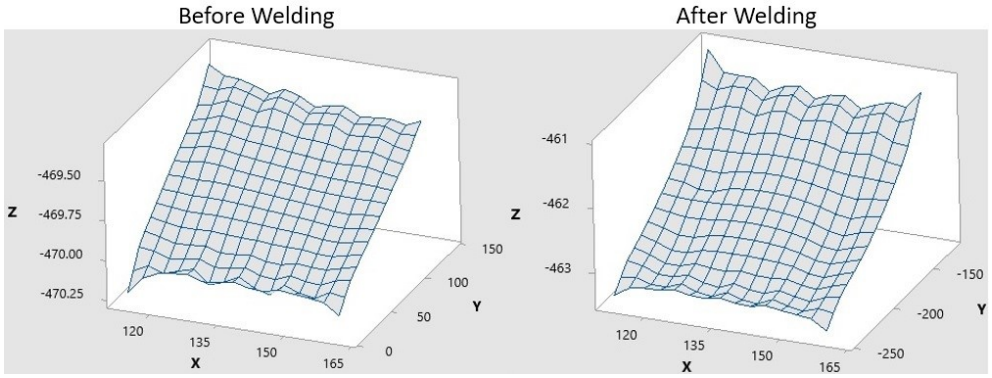

Figure 13. Surface behavior in cartesian coordinates - specimen DWT13.

Figure 14. Overlap deformation - specimen DWT13.

Analysis revealed a tendency for flat dimensions to bend in a parabolic fashion and deviations from straightness caused by residual stresses caused by the welding arc (Figures 5-9). The measuring geometric deviation method before and after flux cored arc welding applied in 304 stainless steel has an important role in ensuring the welds quality. By careful analyses, revision strategies, and precise measurements, we can minimize dimensional variation and ensure part compliance, contributing to final product excellence and satisfaction within required quality controls.

4. CONCLUSIONS

One of the main concerns when welding parts made with the above materials is to avoid deformations and geometric deviations that could impair the quality and functioning of the welded structure. These variations can be

caused by factors such as excessive application of heat during the welding process, residual stresses that develop, material properties, and even variations in part dimensions.

In this work, a linear relationship was not observed between the magnitude of the residual stresses and the welding energy due to competitive phenomena such as the precipitation of δ ferrite in the weld metal and the volume of material deposited when applying the coatings using high heat input. The volume fraction of delta ferrite (within an austenite-ferrite matrix) could possibly have a significant influence on the magnitude of residual stresses.

The reinforcement in the middle of the bead has a greater influence on parallelism (xy and y) and zx squareness and straightness than bead length.

In alloys 18-8 (%Cr-%Ni), there is a greater variation of residual stresses along the width of the weld bead, that is, such fluctuations indicate that the residual stresses are not constant in the irradiated areas.

5. ACKNOWLEDGEMENTS

The authors acknowledge POLI-USP (GMSIE), EEL-USP, UFTM (Mechanical Engineering Department), Miller equipment (FCAW), Soudage (base metal); ITW Welding (tubular wire); COMTEQ Soldas and GULLCO (Welding).

6. REFERENCES

Arun, D., Ramkumar, K. D., Vimala, R., 2019. “Multi-pass arc welding techniques of 12 mm thick Super-duplex stainless steel”. *Journal of Material Process*. Accepted anuscript.https://doi.org/10.1016/j.jmatprotec.2019.03.031.

Barban, L. M.; Gonçalves, E., 2013. Estado da arte da análise de tensões e deformações térmicas devidas à soldagem. 7o COBEF, n. 2008.

Deng, D.; Murakawa, H., 2006. Numerical simulation of temperature field and residual stress in multi-pass welds in stainless steel pipe and comparison with experimental measurements. Computational Materials Science, v. 37, p. 269–277.

Dias, A.O., 2009. Análise da Influência dos Parâmetros de Pulsação na Soldagem do Aço Inoxidável AISI 304 Através do Arame Tubular AWS E316LT1-4. 116p. Dissertação (Mestrado) - Departamento de Mecânica, Universidade Federal de Itajubá, Itajubá, Brazil.

Lippold, J. C.; Kotecki, D. J., 2005. Welding Metallurgy and Weldability of Stainless Steels. [s.l.] John Wiley & Sons, Inc..

Lima, A.C., Ferraresi, V.A., 2006. “Estudo dos Modos de Transferência Metálica de um Arame Tubular Autoprotegido com Variação na Distância Bico de Contato-Peça”, *In: Congresso Nacional de Soldagem - CONSOLDA* 2006. São Paulo, Brazil, pp.164-172.

Marques, P.V. et al., 2005. Soldagem: Fundamentos e Tecnologia, Editora UFMG, Belo Horizonte, 2nd Edition, pp.233-231.

Masubuchi, K. , 1980. Analysis of Welded Structures. [s.l.] Materialls Science and Technology.

Oliveira, L.M., 2005. Uma Investigação da Influência dos Parâmetros de Pulso em Soldagem com Eletrodo Tubular com Proteção Gasosa. 103p. Dissertação (Mestrado) - Departamento de Mecânica, Universidade Federal de Itajubá, Itajubá.

Rong, Y.; Zhang, G.; Huang, Y., 2016. Study of Welding Distorcion and Residual Stress Considering Nonlinear Yield Stress Curves and Multi-constraint Equations. Journal of Materials Engineering and Performance.

Salerno, G. et al. , 2018. On the interaction between welding residual stresses: A numerical and experimental investigation. International Journal of Mechanical Sciences, v. 144, n. May, p. 654–667.

Senatore, M.; Perea, E. , 2007. Ligas Inoxidáveis Estudo comparativo entre os aços inoxidáveis dúplex e os inoxidáveis AISI. Revista Escola de Minas, v. 60, n. 1, p. 175–181.

Sriba, A.; Vogt, J. B.; AMARA, S. E. , 2018. Microstructure, Micro-hardness and Impact Toughness of Welded Austenitic Stainless Steel 316L. Transactions of the Indian Institute of Metals, v. 71, n. 9, p. 2303–2314.

Srivastava, M. et al. , 2018. Residual stress and surface properties of stainless steel welded joints induced by ultrasonic pulsed water jet peening. Measurement: Journal of the International Measurement Confederation, v. 127, n. April, p. 453–462.

Starling, D.M.C., Modenesi, P. J. , 2006. “Avaliação da Transferência de Metal de Arames Tubulares”, Soldagem & Inspeção, Vol.11, No.3, pp.147-155.

Vargas, E., 2019. *Análise das Fraturas em Campos Complexos de Tensão Residual.* Ph.D. thesis, Graduate Program in Mechanical Engineering, Polytechnic School, University of São Paulo, São Paulo, Brasil.

7. RESPONSIBILITY NOTICE

The authors are the only responsible for the printed material included in this paper.